Plant Biotechnology 31, 195–205 (2014)
DOI: 10.5511/plantbiotechnology.14.0331a

Original Paper

High speed and high precision optical interferometric technique to investigate instantaneous growth related changes of plant leaves

Bodhipaksha Lalith Sanjaya Thilakarathne[1], Uma Maheswari Rajagopalan[2], Hirofumi Kadono[1,*], Tetsushi Yonekura[3]

[1]Graduate School of Science and Engineering, Saitama University, Saitama 338-8570, Japan; [2]Laboratory for Integrative Neural Systems, RIKEN Brain Science Institute, Wako, Saitama 351-0198, Japan; [3]Center for Environmental Science in Saitama, Kazo, Saitama 347-0115, Japan
*E-mail: kadono@env.gse.saitama-u.ac.jp Tel & Fax: +81-48-858-3873

Received January 18, 2014; accepted March 31, 2014 (Edited by K. Hiratsuka)

Abstract Instantaneous growth related changes of leaves of Radish, Soybean and rice plants were investigated with a high-speed and ultra-high accuracy optical interferometer. The interferometer, called statistical interferometer, SIT (Statistical Interferometric Technique) is a real-time, non-contact, and robust one and has a subnanometric accuracy and can measure leaf elongation changes every 500 ms. SIT revealed the existence of nanometric fluctuations in the elongation of leaves. Control experiments with dead and mature leaves did indeed establish the existence of null or smaller standard deviations in the fluctuations in contrast to the large deviations obtained for young and healthier leaves. Moreover, the standard deviations of the fluctuations were found to be sensitive to environment of ozone(O_3), a secondary atmospheric pollutant. Long term O_3 exposure with Radish and Soybean leaves led to a decrease in the standard deviations of nanometric fluctuations with increase in O_3 concentrations which correlated with a decrease of gas exchange measures. Under short term O_3 exposures for 3 h with two Japanese rice cultivars, cv. Koshihikari and cv. Fusaotome that are known to have varying O_3 tolerance made the nanometric fluctuations to decrease in comparison to gas exchange measures which showed no variation. The fluctuations could also differentiate the cultivar's sensitivity to O_3 with cv. Koshihikari showing a drastic reduction in comparison to cv. Fusaotome. The results suggest that the nanometric fluctuations may possibly relate to the life maintaining physiological state of the plant and thus may act as an indicator of the vitality of the plant.

Key words: Atmospheric pollution, environmental effects, instantaneous growth, optical interferometry, ozone.

Recently various imaging techniques have been developed to measure plant growth in short-term apart from the conventional dry mass measurements (Kobayashi et al. 1995). Imaging techniques are based on sequential acquisition and processing of images (van der Weele et al. 2003; Walter et al. 2002). However, such image analysis using optical imaging system has a fundamental theoretical limitation determined by the diffraction limit of the wavelength of the light used and thus limited to a few to a few tens of microns. The effect of limitation appears as degraded image which could be worsened further by spatial averaging algorithms used in calculations.

As a way to overcome the limitations and measure plant growth at higher accuracy, attempts were made to use optical interferometer. An optical interferometer involves the interference of coherent light from an optically flat reference mirror and that reflected from a plant. Irrespective of its implementations in 1980's (Briers 1977; Fox and Puffer 1976, 1977; Jiang and Staude 1989), its usage was limited because of two main factors: One was the complexity of the implementation and the other was the optical property of the plant surface and other deeper tissue structures. Plant is a highly scattering object, and the scattered light consists of the light components due to stationary structures and moving

Abbreviations: A_{380}, Net photosynthetic rate at 380 μmol mol^{-1} CO_2 under light saturated conditions of photosynthetic photon flux density 1200 μmol m^{-2} s^{-1}; (ambient*1.5) O_3, Ambient air with 1.5 times concentration of O_3; CCD, Charge Coupled Device; CF, Charcoal Filtered; C_i, Intercellular CO_2 concentration; g_s, Stomatal conductance to water vapour; IF, Interference Filter; NDF, Neutral Density Filter; NIF, Nanometric Intrinsic Fluctuations; NNIF, Normalized Nanometric Intrinsic Fluctuations; OTC, Open Top Chamber; PDF, Probability Density Function; PF, Polarization Filter; PZT, Piezoelectric Transducer; RER, Relative Elongation Rate; SD, Standard Deviation; SD_{after}, Standard Deviation of Relative Elongation Rate after O_3 exposure; SD_{before}, Standard Deviation of Relative Elongation Rate before O_3 exposure; $SD_{exposure}$, Standard Deviation of Relative Elongation Rate during O_3 exposure; SIT, Statistical Interferometric Technique

This article can be found at http://www.jspcmb.jp/
Published online June 17, 2014

scatterers such as organelles within the cells of leaf. Unwanted scattered coherent light leads to the formation of a random pattern, called speckles (Goodman 1984), obstructing the interferometer to achieve the expected accuracy.

While overcoming such technical limitations, and at the same time to achieve a subnanometer accuracy, a novel technique called Statistical Interferometric Technique (SIT) (Kadono et al. 2001; Kadono and Toyooka 1991) has been employed. In SIT, instead of a plane wave generated from an optically flat mirror used in a conventional interferometer (Hariharan 1985), a totally random wavefront or speckle field was used. The speckle, in general, considered as a noise, was utilized as a reference and the interference of speckle patterns was obtained. In addition, the high accuracy was guaranteed through a robust design consisting of prism blocks. The design allowed interfering scattered fields to travel along a common path making the interferometer robust toward external variations.

SIT provides a way to directly conduct observation of plant elongation at nanometric accuracy and thus enabling to look at instantaneous physiological changes that may happen at the cellular level. Based on our preliminary measurements with SIT, random fluctuations in the order of nanometer level were observed during measurements of root of Japanese red pine infected by ectomycorrhizal fungi and were found to be affected by the environment (Rathnayake et al. 2007, 2008). Further, SIT was successfully applied to investigate the effect of illumination conditions on the growth of rice (Kobayashi and Kadono 2010).

In this report the objective was to investigate the reliability of the presence of the random fluctuations and its dependence on environment. As an environmental parameter, the influence of atmospheric pollutant O_3 was chosen. O_3 is known to be a pollutant widely present in the atmosphere causing damage to the plant growth and crop yield (Ainsworth 2008; Ashmore 2005; Darrall 1989). Two set of experiments were done to investigate the random fluctuations accompanying plant growth.

The first set of experiments was done under long term or long term exposures of O_3 to of Radish and Soybean, and was correlated with the gas exchange measures. Radish and Soybean were used as samples due to their importance of being commonly consumed crops, and their high sensitivity to O_3 (Burkey and Carter Jr 2009; Miyake et al. 1989; Nouchi 2002; Yonekura 2005). In the second set of experiments, short term or short term exposure concentrations of 0 ppb, 120 ppb, and 240 ppb for 3 h were used to investigate the validity of SIT under very small dosages of O_3. Leaves of two different rice cultivars based on their differences in yields under O_3 exposure from field studies, namely, cv. Koshihikari and cv. Fusaotome were chosen. Cv. Fusaotome was reported to be more tolerant for O_3 than cv. Koshihikari (Nouchi et al. 2008; Yamaguchi et al. 2011).

Materials and methods

Experiments of long term ozone exposure with Radish and Soybean using open top chamber

All the experiments were conducted with plants grown in open top chambers (OTCs) at Centre of Environmental Science in Saitama, in Saitama pref., Japan. In Saitama prefecture, because of the northern winds flowing from the neighbouring Tokyo region, relatively high concentrations of atmospheric gaseous pollutants including O_3 are found. Soybean (*Glycine max* L. cv. Enrei) and Radish (*Raphanus sativus* L. cv. Kometto) were kept for 30 days in three OTCs (1.8 m×1.8 m×2.4 m). Sample preparation involved the following steps.

For the first 4 days, Soybean and Radish seeds were placed continuously in moist paper towels and germinated at a temperature of 25°C. Seedlings were transplanted to 1.4 l plastic pots (150 mm in depth and 110 mm in diameter) containing black soil with four seedlings per pot. The pots were placed in a chamber supplied with charcoal filtered (CF) air.

After 3 days, the seedlings were exposed to three different concentrations of O_3 namely, CF air, ambient air, and ambient air with 1.5 times concentration of O_3 ((ambient*1.5) O_3) for 30 days from early June to early September of 2012. After O_3 exposure, measurements of conventional gas exchange parameters of net photosynthetic rate, stomatal conductance, and intercellular CO_2 concentration, and SIT were conducted over a duration of 3 days. Six samples of each Soybean and Radish were used for measurements.

Experiments of short term ozone exposure with rice cultivars

Culturing of rice cultivars

This research was carried out in growth chambers at Saitama University. Thirty to forty days old two rice cultivars (*Oryza sativa* L. cv. Koshihikari and cv. Fusaotome) were used. The age of the cultivars was chosen based on earlier studies (Inada et al. 2008; Yamaguchi et al. 2008). Those studies showed that for the cultivars grown under O_3 exposure during the length of vegetative period of around 30 to 40 days, there was a significant reduction on the relative growth rate, net assimilation rate, and photosynthetic rate. Both cultivars were cultured under the following identical conditions.

Seeds of cv. Koshihikari and cv. Fusaotome were pre-germinated in dark environment for 4 days. Both cultivar seedlings were transferred to separate plastic containers (600 ml volume cup) with two plants per container. Half of the container was filled with soil containing clay, humus, and 0.02 g of N-P-K fertilizer in the respective ratio of 14 : 14 : 14. N-P-K fertilizer was used to obtain well developed plants. The containers were placed in a growth chamber (Conviron, Controlled Environmental Ltd., Winnipeg, Canada) during 3 weeks.

A day cycle of the chamber consisted of 12 h at light intensity of 260–350 μmol m^{-2} s^{-1} and 12 h of light intensity of 0 μmol m^{-2} s^{-1}. During the total experimental period of 6 months, air temperature ranged from 18 to 25°C, and the relative humidity ranged from 55 to 65%. Both temperature and humidity were kept constant with variations around ±1°C and ±5%, respectively, during the experiments. Six samples of each cultivar were used for measurements.

Ozone exposure system

The O_3 exposure system consisted of an air pump, charcoal filters, O_3 generator (OES 10A, Dylec Inc., Ami-machi, Japan), O_3 monitor (Model 1150, Dylec Inc., Ami-machi, Japan), and O_3 exposure chamber (0.335×0.335×0.58 m^3). The air from the air pump was passed through a charcoal filter to remove the ambient O_3. The same inlets and outlets in the chamber were used for O_3 and the CF air. O_3 concentrations were monitored with the O_3 monitor, and the signal was fed back to the O_3 generator to maintain the O_3 concentration to be 120 ppb or 240 ppb. The O_3 feedback control system had an accuracy of around 0.5% during the experiment.

O_3 generation system had the rising and falling settling times of 10 and 14 min between 0 and 120 ppb, and between 0 and 240 ppb, respectively. O_3 concentrations used here were chosen based on the common criteria used in Japan. According to the Air Pollution Control Law in Japan (Article 23), the O_3 concentration of 120 ppb corresponds to issuing warning while 240 ppb corresponds to issuing a serious warning.

Timing protocol of Ozone exposure

First, after clamping the leaf of rice plant in the chamber, steady signal acquisition was confirmed. Next, continuous CF air (10 l min^{-1}) was introduced into the chamber for 2 h followed by start of data acquisition. Experiments were done with each experimental session conducted within a day from 11:00 a.m. to 6:00 p.m. The O_3 exposure protocol consisted of the first 1 h with CF air followed by O_3 for next 3 h and CF air was again used to fill the chamber for the last 3 h. O_3 concentrations of control or 0 ppb, 120 ppb, and 240 ppb were used.

Experiments using Statistical Interferometer Technique

Experimental system

A schematic of the statistical interferometer (Figure 1A) shown along with a photograph of the O_3 exposure system (Figure 1B) assembled on an optical bench (Meiritsu seiki, Yokohama, Japan) was used. Only difference for the measurements under long term O_3 exposure with Soybean or Radish was that the no O_3 chamber was used. The light emerged from a He–Ne laser of wavelength 633 nm (GLG 5400, NEC Corporation, Tokyo, Japan) was used as light source. After passing through a neutral density filter (NDF) (F71N-2, Suruga Seiki, Shizuoka, Japan), the laser light was divided into two beams by a specially designed prism P1 (Suruga Seiki, Shizuoka, Japan). These two probing beams perpendicularly illuminated the surface of the target leaf. The target leaf was fixed using a custom-made clamp (Figure 1C). Radish or soybean leaf, and third or fourth of the rice leaf with the length 150 to 200 mm were fixed in the SIT measurement system. During clamping of the leaf, precaution was taken to avoid direct contact with the leaf by using a soft material of cotton at the clamp. The clamp position was set to be around 40 mm from the apex of the leaf.

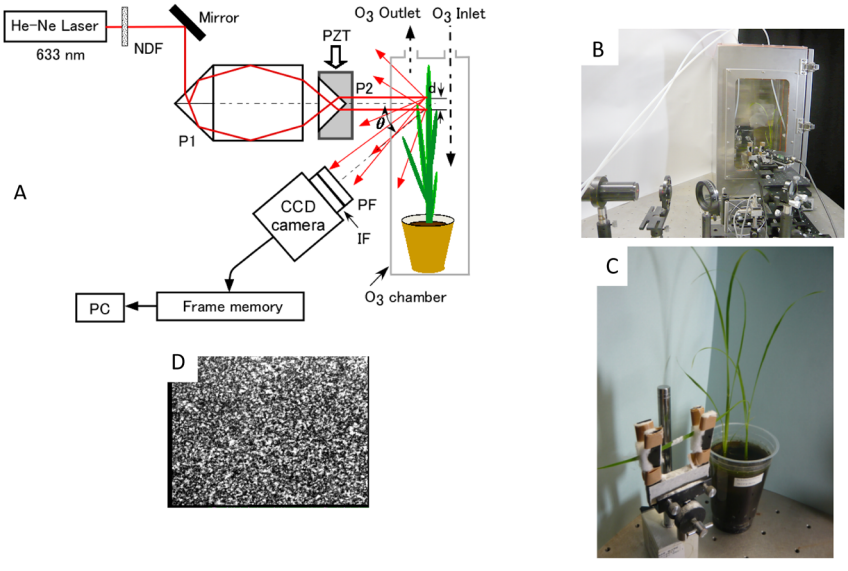

Figure 1. A schematic of the experimental system of SIT (A) used for measuring plant growth placed in an O_3 chamber with a photo of the real system on an optical bench (B) and a stably clamped leaf (C). The camera was placed at a distance of 83 mm from the probing area, and the speckle interference patterns (D) were continuously recorded. IF: interference filter, NDF: neutral density filter, PF: polarization filter, PZT: piezoelectric transducer, P1 and P2: prisms to generate two parallel probing beams, θ: angle between the illuminating and observing directions. Three halogen lamps with fiber optic light guides were used to provide light intensities of 500 μmol m^{-2} s^{-1} from the top of O_3 chamber (not shown in the diagram).

On illuminating two points on the leaf, two independent scattered light field, i.e., speckle fields, were generated that interfered to make a random interference speckle pattern (Figure 1D). The speckle patterns were acquired by a CCD camera (XC-75, Sony Corp., Tokyo, Japan) set at a distance of 83 mm from the leaf at an angle θ=22° to the normal after passing through an interference filter (IF) and polarization filter (PF). Light intensity was adjusted by NDF to be within the dynamic range of CCD camera. A frame grabber (Imperx Vce Pro, Hampshire, UK) was used to acquire and store the interference speckle patterns continuously. The interference filter worked as a band-pass filter and had a central wavelength of 633 nm and a bandwidth of 10 nm. The orientation of PF was adjusted to maximize the interference signal. The distance d between the points of illumination on the leaf could be adjusted by moving the prism P2 (Suruga Seiki, Shizuoka, Japan) mounted on a piezoelectric transducer stage (PZT) (E-620, Physik Instrumente, Karlsruhe, Germany) along the optical axis. The distance d was kept to be the same in all the experiments and was set to be 3 mm. Three halogen lamps with fiber optic light guides (PHL-150, Mejiro Precision Ltd., Tokyo, Japan) were used to provide a light intensity of 500 μmol m^{-2} s^{-1}.

When the probe beam illuminated the surface of the leaf, the light also penetrated into the leaf. Light penetration would result in the generation of dynamic speckles from moving organelles. Such speckles also known as biospeckles (Aizu and Asakura 1996) would degrade the measurement accuracy of SIT. Therefore, to avoid light penetration into the leaf, the probing area was covered with wheat flour.

In order to investigate the effect of light penetration through wheat flour, the amount of light transmitted through the flour layer was measured and it was found to be 2% of the incident light. The light penetrated into the leaf through the flour layer would form biospeckles on the CCD camera. However, the amount of light involved in the formation of the biospeckles was much less than 0.04% of the incident probing beam as the incident light and the light scattered back passed through the same flour layer. The effect of flour such as the displacement from the flour particles in the measurement of nanometer displacements were found to be very small (details given in supplementary information S4).

Actually, the wavelength of 633 nm of He–Ne laser used in the experiment was very close to the absorption band of chlorophyll a and b in spite of the penetrated light power being fairly small. Two additional experiments were performed in order to confirm the effect of the wavelength. In the first experiment, a laser of wavelength 532 nm of YAG-SHG (Second Harmonic Generation) laser (CL532-100-S, CrystaLaser, Reno, USA) was employed (supplementary information S5).

In the second experiment, an additional beam having the same wavelength as the probing beam was used. A larger powered light illuminated the backside of the probing area with the power corresponding to double the value P_t. The leaf elongation was measured by turning on and off the additional beam every 2 h. The results obtained showed that there was no effect due to the additional illumination. Details are given in supplementary information S6. Thus, a leakage of 2% of the probing beam did not affect the measurements. So by taking into account of this leakage, the incident power of the probing beam was kept constant during the experiment.

Principle of statistical interferometric technique

SIT is a non-contact optical interferometric technique for measuring displacements at an accuracy of subnanometer and has a temporal resolution of 500 ms (Kadono et al. 2001; Kadono and Toyooka 1991). Principle of statistical interferometry is different from that of conventional interferometric techniques. In a conventional interferometer (Hariharan 1985), the light reflected from an optically flat reference mirror and the reflected light from the sample under observation interfere to give an interference pattern. The phase change is derived from the interference pattern. It corresponds to the change of the optical path such as a displacement of the sample. In order to achieve subnanometer accuracy, stringent conditions were imposed on the reference arm to make the resulting reference wavefront with no uncertainty such as deformity of reference mirror.

In contrast, a completely random wavefront called a fully developed speckle field is used in SIT as a reference and is generated when an optically rough surface is illuminated by a laser light. In SIT, this random field is used as a reference. Phase of the speckle field has a uniform probability density function (PDF) that takes a constant probability density of $1/2\pi$ over the phase range from $-\pi$ to π. Characteristics of the speckle phase is remarkably stable and reliable and can play the role of a standard. To understand the principle of this method, it is necessary to have an understanding of the fundamental properties of the speckle fields and their statistics that are given in supplementary information S1.

In SIT, two points on the leaf were illuminated perpendicularly by the probing beams, and two independent speckle fields were generated. These fields interfered to make a random interference speckle pattern. The speckle patterns were acquired by a CCD camera for every 500 ms and stored in a frame memory. Basically, when there is an elongation of Δx between the two illuminating points of the object, the optical path difference ΔL between the two interfering speckle fields can be expressed by,

$$\Delta L = \Delta x \sin\theta, \tag{1}$$

where θ is the angle between the illumination and the observation directions. Due to the elongation Δx, the phase difference between the two interfering light fields changes by Ψ and is given in terms of ΔL as

$$\Psi = (2\pi / \lambda)\Delta L. \tag{2}$$

Calculation of leaf elongation and elongation rate

In our SIT algorithm, for deriving the unknown object phase

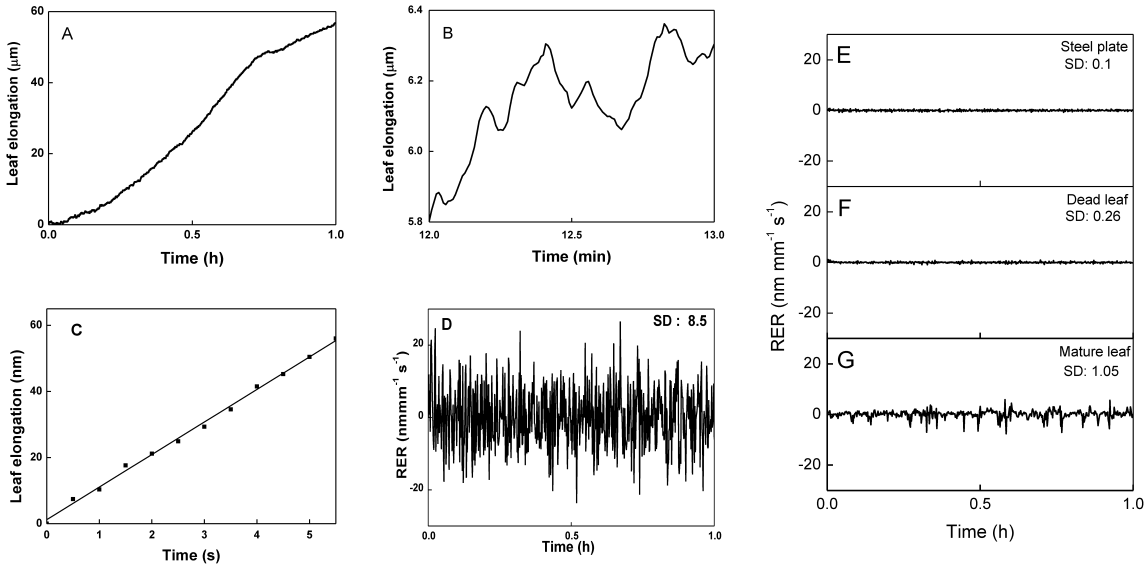

Figure 2. Leaf elongation of rice was continuously measured over 7 h and shown at different time scales (A–C). Relative leaf elongation rate (RER) for the leaf (D) shown along with the system fluctuations measured with a metal plate (E), a dead leaf (F), and a mature leaf (G). The results were shown for an hour (A), a minute (B), and a few seconds (C). In (C), the straight line corresponded to a linear regression done to obtain the leaf elongation rate.

Ψ, the statistical property of the speckle phase, i.e., the total randomness of the speckle phase was used as a constraint. A detailed basic SIT algorithm, and its extension developed by the authors, and derivation of the unknown object phase are given in Supplementary informations S2 and S3. The whole processing could be performed in real time to get the object phase with very high accuracy.

From the derived leaf elongation over a period τ of 5.5 s, the slope of the elongation data was obtained by linear regression. Relative leaf elongation rate (RER) (nm mm^{-1} s^{-1}) was defined by,

$$\mathrm{RER} = \mathrm{Elongation} / \tau d. \quad (3)$$

RER was calculated over the whole duration of 7 h. These values were used to quantify the influence of O_3 exposure on Radish, Soybean, and two rice cultivars (cv. Koshihikari and cv. Fusaotome). It should be noted here that, in this study, the main focus was given to a local leaf elongation dynamics rather than 'growth' in conventional sense where the displacement of the apex of the leaf is measured from its base.

Error sources and noise level of the measurement system

When SIT is applied to measure the leaf elongation, a specific problem, a decorrelation between speckle patterns which leads to a measurement error, may arise due to slight change of the surface height profile of the leaf. Because the speckle field is generated as a result of random interference of many elementary waves scattered from the leaf surface, the speckle field was affected by a change of surface structure of the leaf in the scale of wavelength. Consideration on this decorrelation is given in the Supplementary information S4. As demonstrated by the experiment described in Supplementary information S4 (Figure S6), the correlations between the speckle patterns were fairly well maintained over a few minutes. This implies that the effect of the decorrelation of the speckle patterns was significantly small in the determination of the elongation rate of the plant leaf.

Next, the noise level of the measurement system of SIT was examined. Measurements were conducted by replacing the plant leaf with a steel metal plate. The metal plate showed small RER fluctuations (Figure 2E). The standard deviation of the fluctuations for the metal plate was 0.1 nm mm^{-1} s^{-1}. The extremely small fluctuations observed for the stationary plate were coming from electronic noise and small system vibrations that could not be eliminated, i.e., noise level of the measurement system. For a relatively large leaf elongation of a few microns to hundreds microns, repeatability of the measurement using SIT was also demonstrated in our previous study (Kobayashi and Kadono 2010).

In addition, the robust optical arrangement and frequent renewal of the reference speckle patterns of the measurement algorithm guaranteed the accuracy of the measurements (Supplementary information S3). The data processing unit of the measurement software was designed so as to continuously monitor invalid data points in the acquired images and to report the number of invalid data points which were mainly due to the decorrelation of speckle patterns and electronic noise.

Data analysis

The data were acquired for 7 h under control and O_3 exposure. The following procedure was applied to obtain the RER and its fluctuations: (a) Linear regression was done over 5.5 s to obtain slope or to obtain instantaneous RER; (b) repetition of procedure (a) for every 5.5 s across the whole session of 7 h;

(c) calculated RER was passed through a moving average filter with window size 165 s to obtain smoothened data; (d) the smoothened data was subtracted out from the RER data of step (b) to eliminate the long-term trend.

In the following sections, special attention was paid to the short-term fluctuations in nanometric scale of RER of the leaf, and was referred to as nanometric intrinsic fluctuations (NIF). In order to characterize NIF, first the commonly employed power spectrum analysis was carried out (Papoulis 1984). The slope of the power spectrum was found to be almost -2 and that means NIF obeyed the power law irrespective of O_3 concentrations.

A moving average filter with a window size of 165 s corresponded to a low pass filter with a cut off frequency of 0.0060 Hz (above procedure (c)). The operation (d) of the above procedure was equivalent to high-pass filtering. Because of the very low cut-off frequency of the filter, most part of the power spectral distribution was not affected by the filtering operation. However, there were changes only in the absolute magnitude of the power spectrum depending on different O_3 concentrations and species of plant. These changes in the magnitude of the spectra could be evaluated using the standard deviation (SD) of the fluctuations.

A parameter called normalized NIF (NNIF) was introduced to characterize NIF. Normalization was done to reduce the common variations during a single session for a sample as well as for different samples. To calculate NNIF, first the standard deviation of NIF was calculated respectively, under the initial 1 h of CF air, SD_{before}, under 3 h of O_3 exposure, $SD_{exposure}$, and under the last 3 h of CF air exposure, SD_{after}, for each sample of each cultivar. Next, $SD_{exposure}$ and SD_{after} were normalized by SD_{before} to give NNIF.

All calculations were done with Matlab (R2011b, MathWorks, Natick, USA). To analyze the statistical significance of the standard deviations obtained under different concentrations of O_3 and for different cultivars, *t*-test was used.

Gas exchange measurements

For comparisons of the RER results obtained under O_3 by SIT, conventional gas exchange parameters that characterized the effect of O_3 were also measured using a portable photosynthesis measurement system (LI-6400, Li-Cor Inc., Lincoln, USA). For measuring the net photosynthetic rate A_{380} that is defined at CO_2 concentration of 380 μmol mol^{-1} (380 ppm) under light saturated conditions of photosynthetic photon flux density 1200 μmol m^{-2} s^{-1}, stomatal conductance to water vapour g_s, and intercellular CO_2, C_i, under light saturated conditions, six plants were selected randomly from each crop. Eight measurements were done for each plant. During the measurements of A_{380}, g_s, and C_i, CO_2 concentration, the air temperature, and the photosynthetic photon flux density in leaf chamber were maintained respectively at 380 μmol mol^{-1}, 25°C, and, 1200 μmol m^{-2} s^{-1}. For the case of rice cultivars, measurements of A_{380} and g_s were conducted before and after O_3 exposure with third or fourth leaf.

Results and discussion

Measurements by statistical interferometric technique

The leaf elongation data were obtained with young rice plants (30 to 40 days old) by SIT (Figure 2A–D). Over 1 h, the leaf elongation was monotonically increasing in the order of a few tens of μm (Figure 2A). Within a minute, the leaf elongation showed random oscillations of a few hundreds of nanometer (Figure 2B). Finally, within 5.5 s, the leaf elongation was almost linear, and the slope represented the average leaf elongation rate within 5.5 s (Figure 2C).

RER was calculated by using Eq. (3) across the total measurement period of 1 h, and the leaf elongation rate revealed fluctuations (Figure 2D). The metal plate showed very small fluctuations in RER (Figure 2E). The SD of the fluctuations for the metal plate was more than eighty times smaller (0.1 nm mm^{-1} s^{-1}) than that for the young leaf. Further, the SD of the fluctuations observed in young leaves was much larger than that of mature leaf that was around 3 months old (Figure 2G) and dead leaf (Figure 2F). SD of dead leaf was closer to that of metal plate. These results suggested that the fluctuations were clearly associated with the physiological state of the plant, i.e., alive or dead. Here dead leaf was referred to as one that had lost its green colour and turned brown becoming dry and stiff.

Fluctuations in RER were observed in different plants species such as Soybean and Radish sprouts (Figure 3). Depending on the plants, the fluctuations varied and had different amplitudes. Representative examples of the RER obtained for Radish and Soybean were shown under different O_3 concentrations of CF air, ambient air, and (ambient*1.5)O_3. Comparing the SDs of the fluctuations revealed that Radish was much larger (around three times) than that for Soybean in all the cases. Further, comparison with the SDs of the fluctuations for rice cultivars revealed that they were largely different as well (data not shown explicitly).

The measured random fluctuations were not just noise from the measurement system but arising out of spatial expansions happening at very fine scales across the leaf. The results showed the possibility that the nanometric RER fluctuations might be an intrinsic property of the plant and were not due to any external factors reflecting the microscopic processes.

On the possible origin of nanometric intrinsic fluctuations

Reason for the presence of nanometric fluctuations is not yet clear. Here we consider the possible factors that might be involved in such fluctuations. When plants were measured at high resolution, the growth rate was fast varying in nm mm^{-1} s^{-1}, and this fast variation could be

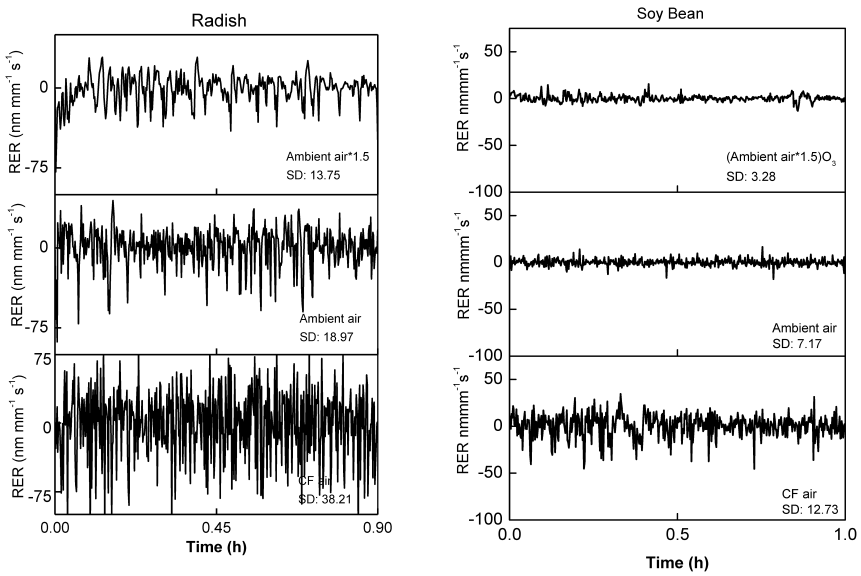

Figure 3. Results of average RER for Radish and Soybean. Top, middle, and bottom rows, respectively, represent the variations obtained under CF air, ambient air and (ambient*1.5) O_3 exposures. Average was obtained of six samples and SD indicates the standard deviations.

observed in different plants including Radish, Soybean and rice cultivars reported here. This fact compels one to hypothesize that these fluctuations could be an intrinsic property of the plant reflecting the microscopic processes.

Growth processes are regulated in the plant on a plethora of system levels, ranging from biomechanical restraints (Niklas 1999) governing leaf form to the endogenous genetic control at the transcriptome level in roots and leaves (Matsubara et al. 2006) and finally on a whole system level by long-range signals. It is also known from the earlier reports about the existence of diel patterns or circadian rhythm in the growth rate of roots and leaves in plants (Dodd et al. 2005; Poiré et al. 2010; Ruts et al. 2012; Schurr et al. 2006; Walter and Schurr 2005).

Carbohydrate metabolism is believed to play an important role in the control of leaf growth. Carbohydrates are the products of photosynthesis, and they are the building blocks of cell wall polymers and provide energy for growth activities (Smeekens et al. 2010). Apart from this metabolic process, hydraulic control mechanism of the leaf includes: expansion and stiffening of the cell wall due to lignin, the activity of transmembrane proteins such as aquaporin that are believed to be regulating the water flow across cells and other parts of the plant by regulating hydraulic conductance and turgor pressure of the cell surface layers (Pantin et al. 2011; Roelfsema and Hedrich 2005). All these dynamic regulatory mechanisms could lead to small-scale expansion processes giving rise to strong mechanical strains inside the growing tissues. Such small-scale changes in local expansion are highly relevant in the context of instantaneous growth dynamics measurement.

As part of the ongoing investigation on the origin, preliminary experiments were done by disrupting hydraulic process (unpublished result). Under the inhibition of aquaporin, the growth rate of Chinese chives was measured. In order to inhibit aquaporin, the root of the plant was dipped into 0.2 mM of $HgCl_2$. NIF measured showed a reduction by half. This result suggests for the possibility of partial involvement of hydraulic process regulating water flow behind the origin of nanometric fluctuations. We expect a detailed study controlling different physiological factors may provide knowledge about the origin of the nanometric fluctuations.

Our understanding of cell wall growth at the cellular and molecular level is very limited (Cosgrove 2000). For the elongation of plant leaves to happen, the cells must physically expand their restraining walls. At the same time, the cell wall must preserve its mechanical integrity in the presence of high turgor pressures. Such competing mechanisms involved may possibly give rise to very fine spatial fluctuations.

Further, cell wall enlargement also follows two different time scales with one undergoing in the order of days to months while the other follows a variation from seconds to hours. The fast trends are superposed on slow trends. In general, the fast variations changes were difficult to measure (1) due to the lack of resolving power of microscopy and (2) due to the lack of revealing power of the real structural arrangement by spectroscopic methods. Spectroscopic methods can identify the bulk polymer conformation and their interaction with the intact wall. With SIT, both the slow and fast variations could be measured.

Nanometric Intrinsic Fluctuations under long term exposure and comparison

In order to validate the nanometric fluctuations, the averaged standard deviations of NIF of RER were calculated under different O_3 treatment of CF air, ambient air, and (ambient*1.5)O_3 for both plant species, Radish and Soybean, and compared with gas exchange measures. Figure 4A–C showed respectively the results of NIF, net photosynthetic rate, A_{380}, and stomatal conductance, g_s.

For both Radish and Soybean, the SDs of averaged NIF obtained under ambient air and (ambient*1.5)O_3 showed significant reductions in comparison to that obtained under CF air. It can be seen that there is a consistent reduction in NIF for both plant species with respect to the O_3 presence. Further, the reductions in the SD between CF air and ambient air, between CF air and (ambient*1.5)O_3 were all statistically significant within $p<0.05$. The reductions in A_{380} and g_s could also be seen for both plant species as the concentration of O_3 increases (Figure 4B, C).

There was consistent decrease in NIF with increasing O_3 concentrations. A fairly good agreement between the SD of NIF and gas exchange measures suggests that NIF obtained using SIT is a valid physiological measure, in spite of being only a point measurement on the leaf surface.

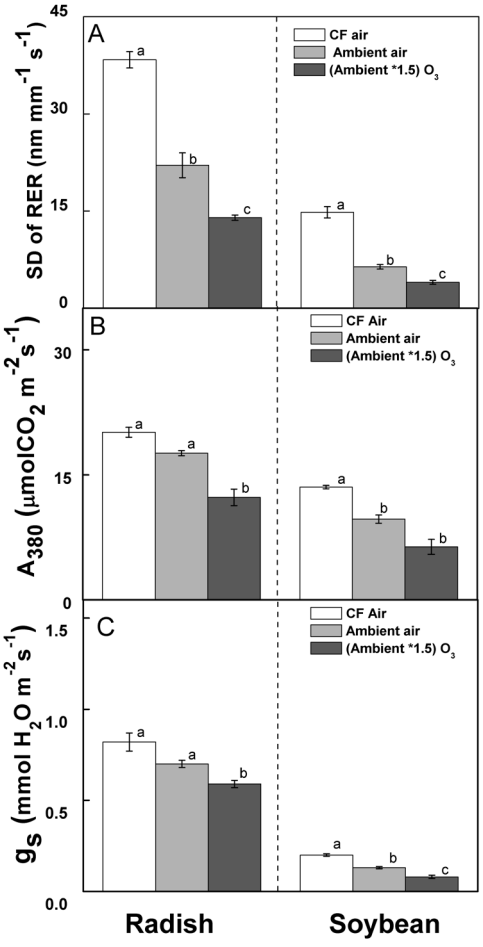

Figure 4. Results of standard deviation of RER (A), net photosynthetic rate A_{380} (B), and stomatal conductance g_s (C) under three different treatments of CF air, ambient air and (ambient*1.5) O_3 for radish and soybean. The error bars correspond to the standard error obtained of six replicates. 'a', 'b' and 'c' correspond to significant differences ($p<0.05$).

Nanometric Intrinsic Fluctuations under short term exposure and comparison

For each of the rice cultivars (cv. Koshihikari and cv. Fusaotome), averaged NNIF was calculated from normalized values of NIF and were shown as a function of time under different O_3 concentrations of 0 ppb, 120 ppb, and 240 ppb in Figure 5. As seen from the results, under control (0 ppb), the averaged NNIF was almost constant for both cultivars. Under O_3 exposures of 120 ppb and 240 ppb, drastic reductions in the averaged NNIF were found immediately during O_3 exposure period for both cultivars.

For cv. Koshihikari, compared to 0 ppb the reduction percentages for 120 ppb and 240 ppb were, respectively, 34% and 40%. In contrast, for cv. Fusaotome, the reduction percentages for 120 ppb and 240 ppb were, respectively, 16% and 22%. Statistical analysis showed

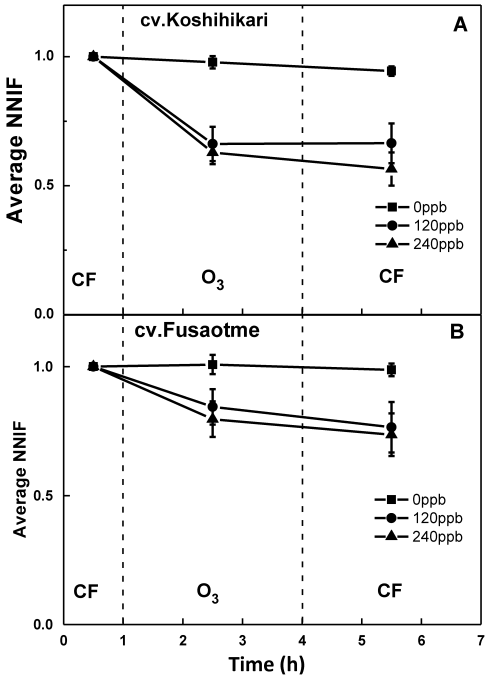

Figure 5. Averaged normalized nanometric intrinsic fluctuations (NNIF) shown for cv. Koshihikari (A) and cv. Fusaotome (B) under O_3 concentrations of 0 ppb, 120 ppb, and 240 ppb. The error bars correspond to standard error obtained of six replicates. Charcoal filtered (CF) air was fed into the chamber for the first 1 h and the last 3 h. O_3 exposure was done for 3 h. Statistically significant differences (*t*-test with $p<0.01$) were obtained between CF air before O_3 exposure and during O_3 exposure for both O_3 concentrations of 120 ppb and 240 ppb in both cultivars.

a significant difference ($p<0.01$) for both cultivars, between control and 120 ppb exposure, and control and after 120 ppb exposure. This was true for 240 ppb too. Comparing the averaged NNIF obtained after O_3 exposure with those obtained during the exposure the reduction was small under the different concentrations of 120 ppb and 240 ppb and also for both cultivars. The results showed that the immediate influence which occurred in the leaf due to O_3 exposure was large.

The results of net photosynthetic rate A_{380} (top row), stomatal conductance g_s (middle row), and intercellular CO_2 concentration C_i (bottom row) for cv. Fusaotome (left column) and cv. Koshihikari (right column) are shown in Figure 6. C_i that is indirectly related to the O_3 exposure did not show any difference for both cultivars. For the case of cv. Fusaotome, apart from C_i, both A_{380} and g_s also showed no difference on exposure to O_3. On the other hand, for cv. Koshihikari, both A_{380} and g_s decreased. The significant decrease in g_s suggested that the stomatal closure would lead to decrease in photosynthesis. This result agreed with the decrease in nanometric fluctuations. Comparison results were given only for 240 ppb. For 120 ppb, the gas exchange parameters, did not show any difference against control (data not shown).

In short term O_3 exposure experiments with rice, cultivars that were known to have different tolerances to O_3 (Nouchi et al. 2008; Yonekura 2011) were used. The difference between the cultivars toward O_3 was consistent with the post-harvest yields measured over 4 months (Yamaguchi et al. 2008). Exposure of relatively very small dosages of O_3 concentrations of 120 ppb and 240 ppb

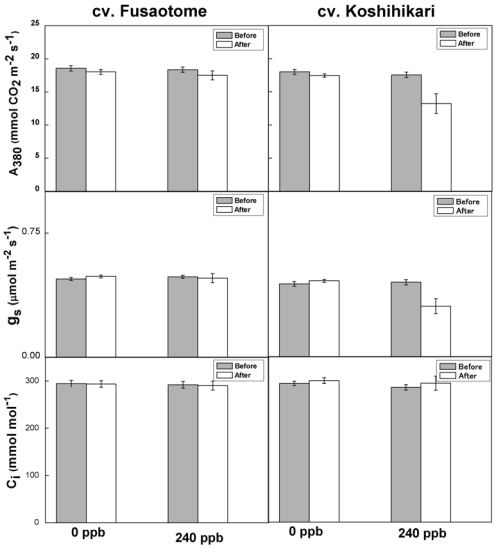

Figure 6. Leaf net photosynthetic rate A_{380}, stomatal conductance g_s (middle column), and intercellular CO_2 concentration C_i for cv. Fusaotome (top row) and cv. Koshihikari (bottom row) obtained under O_3 concentrations of 0 ppb and 240 ppb. The error bars correspond to standard error obtained of six replicates.

for a short duration of 3 h in 1 day was found to make a difference in the magnitude of fluctuations (Figure 5). Therefore, relatively small dosages were enough to induce reduction of the fluctuations proving the relatively very high sensitivity of SIT measurement as compared to gas exchange measures (Figure 6).

Actually, gas exchange measures under 120 ppb could not show a significant changes (Figure 6). Only net photosynthetic rate A_{380} and stomatal conductance g_s showed significant reductions by 25% and 32%, respectively, for cv. Koshihikari at 240 ppb. In case of cv. Fusaotome, no changes were detected in the gas exchange parameters of A_{380} and g_s, and the changes in the averaged NNIF was half of that for cv. Koshihikari (Figure 5). These facts suggest that the conventional gas exchange parameters for assessing the effect of O_3 are not sensitive enough toward O_3 especially to detect O_3 tolerant cultivars under small dosages of O_3 concentrations.

Ozone concentration and sensitivity of nanometric intrinsic fluctuations

In order to explain the reduction of fluctuations in RER under exposure to O_3, first we consider the effects of O_3 on plants. With O_3 exposure, both the photosynthetic rate and the stomatal conductance decreased. The reduction in photosynthetic rate may be correlated to the slowdown of the dark reactions of the Calvin cycle, mainly due to the loss of Rubisco activity (Fiscus et al. 2005; Guidi et al. 2007; Miller et al. 1999) and stomatal limitations (Reid and Fiscus 1998). Moreover, O_3 results in structural changes of cell possibly cell death leading to reduction in growth (Rao and Davis 1999; Wiese and Pell 2003).

Further, the O_3 induced reactive oxygen species superoxide anions, hydroxyl radicals, and hydrogen peroxide may damage membrane lipids, proteins and nucleic acids (Inada et al. 2008; Sharma et al. 1996). This in turn may lead to water loss, wilting and withering (Yue-ming et al. 2004) and thus resulting in reducing possible growth fluctuations at scales of nm. Exposure to O_3 results in the reduction of physiological processes, namely metabolic and hydraulic processes (Black et al. 2007; Kangasjärvi et al. 2005; Rao and Davis 2001; Roelfsema and Hedrich 2005; Ruts et al. 2012; Wilkinson and Davies 2010).

In SIT, the measured NIF decreased for all Radish, Soybean and rice cultivars agreeing with the reduction of gas exchange parameters A_{380} and g_s. Existence of correlation under long-term O_3 exposure between the gas exchange parameters A_{380} and g_s and the averaged SD of NIF suggests for the involvement of the metabolic factors. In case of rice cultivar exposed to 3 days of at a concentration of 240 ppb, actual visible damages in leaves could be observed after about 1 week of O_3 exposure

(Thilakarathne et al. 2014).

In summary, SIT offers a complementary, feasible, promising and high sensitivity measurement technique that has the capability of providing new insights on the dynamics of plant growth related processes at subnanometer accuracy. The NIF discovered here were found to be not only correlated with the conventional O_3 assessment parameters but also more sensitive to smaller O_3 concentrations. NIF could also differentiate the O_3 tolerance of cultivars where the conventional methods of O_3 assessment failed to respond. The results could be significant as NIF would provide a much faster way of assessment for O_3 stress. The NIF seemed to reflect a fundamental process in regulating the plant growth dynamics at the microscopic level, and a clarification of the real physical origin behind the presence of the nanometric intrinsic fluctuations requires further research.

Acknowledgements

This work was partly supported by the Grant-in-Aid for Science Research in JSPS (22310026) of the Ministry of Education, Culture, Sports, Science and Technology in Japan.

References

Ainsworth EA (2008) Rice production in a changing climate: A meta-analysis of responses to elevated carbon dioxide and elevated ozone concentration. *Glob Change Biol* 14: 1642–1650

Aizu Y, Asakura T (1996) Bio-speckles. In: Consortini A (ed) *Trends in Optics*. Academic Press, San Diego, pp 27–49

Ashmore MR (2005) Assessing the future global impacts of ozone on vegetation. *Plant Cell Environ* 28: 949–964

Black VJ, Stewart CA, Roberts JA, Black CR (2007) Ozone affects gas exchange, growth and reproductive development in *Brassica campestris* (Wisconsin Fast Plants). *New Phytol* 176: 150–163

Briers JD (1977) The measurement of plant elongation rates by means of holographic interferometry: Possibilities and limitations. *J Exp Bot* 28: 493–506

Burkey KO, Carter Jr TE (2009) Foliar resistance to ozone injury in the genetic base of U.S. and Canadian soybean and prediction of resistance in descendent cultivars using coefficient of parentage. *Field Crops Res* 111: 207–217

Cosgrove DJ (2000) Expansive growth of plant cell walls. *Plant Physiol Biochem* 38: 109–124

Darrall NM (1989) The effect of air pollutants on physiological processes in plants. *Plant Cell Environ* 12: 1–30

Dodd AN, Salathia N, Hall A, Kévei E, Tóth R, Nagy F, Hibberd JM, Millar AJ, Webb AAR (2005) Plant circadian clocks increase photosynthesis, growth, survival, and competitive advantage. *Science* 309: 630–633

Fiscus EL, Booker FL, Burkey KO (2005) Crop responses to ozone: Uptake, modes of action, carbon assimilation and partitioning. *Plant Cell Environ* 28: 997–1011

Fox MD, Puffer LG (1976) Analysis of transient plant movements by holographic interferometry. *Nature* 261: 488–490

Fox MD, Puffer LG (1977) Holographic interferometric measurement of motions in mature plants. *Plant Physiol* 60: 30–33

Goodman JW (1984) Statistical properties of laser speckle patterns. In: Dainty JC *Laser Speckle and Related Phenomena* (*Topics in Applied Physics*). Springer-Verlag, Berlin, pp 9–75

Guidi L, Mori S, Degl'Innocenti E, Pecchia S (2007) Effects of ozone exposure or fungal pathogen on white lupin leaves as determined by imaging of chlorophyll a fluorescence. *Plant Physiol Biochem* 45: 851–857

Hariharan P (1985) *Optical interferometry*. Academic press, Sydney

Inada H, Yamaguchi M, Satoh R, Hoshino D, Nagasawa A, Negishi Y, Nouchi I, Kobayashi K, Izuta T (2008) Effects of ozone on photosynthetic components and radical scavenging system in leaves of rice (*Oryza sativa* L.). *J Agric Meteorol* 64: 243–255

Jiang Z, Staude W (1989) An interferometric method for plant growth measurements. *J Exp Bot* 40: 1169–1173

Kadono H, Bitoh Y, Toyooka S (2001) Statistical interferometry based on a fully developed speckle field: An experimental demonstration with noise analysis. *J Opt Soc Am A* 18: 1267–1274

Kadono H, Toyooka S (1991) Statistical interferometry based on the statistics of speckle phase. *Opt Lett* 16: 883–885

Kangasjärvi J, Jaspers P, Kollist H (2005) Signalling and cell death in ozone-exposed plants. *Plant Cell Environ* 28: 1021–1036

Kobayashi K, Kadono H (2010) Expansion of the dynamic range of statistical interferometry and its application to extremely short- to long-term plant growth monitoring. *Appl Opt* 49: 6333–6339

Kobayashi K, Okada M, Nouchi I (1995) Effects of ozone on dry matter partitioning and yield of Japanese cultivars of rice (*Oryza sativa* L.). *Agric Ecosyst Environ* 53: 109–122

Matsubara S, Hurry V, Druart N, Benedict C, Janzik I, Chavarría-Krauser A, Walter A, Schurr U (2006) Nocturnal changes in leaf growth of Populus deltoides are controlled by cytoplasmic growth. *Planta* 223: 1315–1328

Miller JD, Arteca RN, Pell EJ (1999) Senescence-associated gene expression during ozone-induced leaf senescence in Arabidopsis. *Plant Physiol* 120: 1015–1024

Miyake H, Matsumura H, Fujinuma Y, Totsuka T (1989) Effects of low concentrations of ozone on the fine structure of radish leaves. *New Phytol* 111: 187–195

Niklas KJ (1999) A mechanical perspective on foliage leaf form and function. *New Phytol* 143: 19–31

Nouchi I (2002) Responses of whole plants to air pollutants. In: Omasa K *Air pollution and plant biotechnology*. Springer-Verlag, Tokyo

Nouchi I, Kobayashi K, Izuta T (2008) Effects of ozone on the growth, yield and leaf gas exchange rates of two japanese cultivars of rice (*Oryza sativa* L.). *J Agric Meteorol* 64: 131–141

Pantin F, Simonneau T, Rolland G, Dauzat M, Muller B (2011) Control of leaf expansion: A developmental switch from metabolics to hydraulics. *Plant Physiol* 156: 803–815

Papoulis A (1984) *Probability, Random Variables and Stochastic Processes*. Mc-graw-Hill, Singapore

Poiré R, Wiese-Klinkenberg A, Parent B, Mielewczik M, Schurr U, Tardieu F, Walter A (2010) Diel time-courses of leaf growth in monocot and dicot species: Endogenous rhythms and temperature effects. *J Exp Bot* 61: 1751–1759

Rao MV, Davis KR (1999) Ozone-induced cell death occurs via two distinct mechanisms in Arabidopsis: The role of salicylic acid. *Plant J* 17: 603–614

Rao MV, Davis KR (2001) The physiology of ozone induced cell death. *Planta* 213: 682–690

Rathnayake AP, Kadono H, Toyooka S, Miwa M (2007) Statistical interferometric investigation of nano-scale root growth: Effects

of short-term ozone exposure on ectomycorrhizal pine (*Pinus densiflora*) seedlings. *J For Res* 12: 393–402

Rathnayake AP, Kadono H, Toyooka S, Miwa M (2008) A novel optical interference technique to measure minute root elongations of Japanese red pine (*Pinus densiflora* Seibold & Zucc.) seedlings infected with ectomycorrhizal fungi. *Environ Exp Bot* 64: 314–321

Reid CD, Fiscus EL (1998) Effects of elevated [CO_2] and/or ozone on limitations to CO_2 assimilation in soybean (*Glycine max*). *J Exp Bot* 49: 885–895

Roelfsema MRG, Hedrich R (2005) In the light of stomatal opening: New insights into 'the Watergate'. *New Phytol* 167: 665–691

Ruts T, Matsubara S, Wiese-Klinkenberg A, Walter A (2012) Diel patterns of leaf and root growth: Endogenous rhythmicity or environmental response? *J Exp Bot* 63: 3339–3351

Schurr U, Walter A, Rascher U (2006) Functional dynamics of plant growth and photosynthesis—from steady-state to dynamics—from homogeneity to heterogeneity. *Plant Cell Environ* 29: 340–352

Sharma YK, Leon J, Raskin I, Davis KR (1996) Ozone-induced responses in *Arabidopsis thaliana*: The role of salicylic acid in the accumulation of defence-related transcripts and induced resistance. *Plant Biol* 93: 5099–5104

Smeekens S, Ma J, Hanson J, Rolland F (2010) Sugar signals and molecular networks controlling plant growth. *Curr Opin Plant Biol* 13: 273–278

Thilakarathne BLS, Rajagopalan UM, Kadono H, Yonekura T (2014) An optical interferometric technique for assesssing ozone induced damage and recovery under cumulative exposures for a Japanese rice cultivar. *SpringerPlus* 3: 89

van der Weele CM, Jiang HS, Palaniappan KK, Ivanov VB, Palaniappan K, Baskin TI (2003) A new algorithm for computational image analysis of deformable motion at high spatial and temporal resolution applied to root growth. Roughly uniform elongation in the meristem and also, after an abrupt acceleration, in the elongation zone. *Plant Physiol* 132: 1138–1148

Walter A, Schurr U (2005) Dynamics of leaf and root growth: Endogenous control versus environmental impact. *Ann Bot (Lond)* 95: 891–900

Walter A, Spies H, Terjung S, Küsters R, Kirchgeßner N, Schurr U (2002) Spatio-temporal dynamics of expansion growth in roots: automatic quantification of diurnal course and temperature response by digital image sequence processing. *J Exp Bot* 53: 689–698

Wiese CB, Pell EJ (2003) Oxidative modification of the cell wall in tomato plants exposed to ozone. *Plant Physiol Biochem* 41: 375–382

Wilkinson S, Davies WJ (2010) Drought, ozone, ABA and ethylene: New insights from cell to plant to community. *Plant Cell Environ* 33: 510–525

Yamaguchi M, Inada H, Satoh R, Hoshino D, Nagasawa A, Negishi Y, Sasaki H, Nouchi I, Kobayashi K, Izuta T (2008) Effects of ozone on the growth, yield and leaf gas exchange rates of two Japanese cultivars of rice (*Oryza sativa* L.). *J Agric Meteorol* 64: 131–141

Yamaguchi M, Inada H, Satoh R, Hoshino D, Nagasawa A, Negishi Y, Sasaki H, Yonekura T (2011) Examination of critical levels of tropospheric ozone for the yield of Japanese rice cultivars. *APGC Symposium* 8: 129–130

Yonekura T (2011) Examination of critical levels of tropospheric ozone for the yield of Japanese rice cultivars. *APGC Symposium* 8: 129–130

Yonekura T, Kihara T, Shimada T, Miwa M, Arzuate A, Izuta T, Ogawa K (2005) Impact of O_3 and CO_2 enrichment on growth of Komatsunas (Brassica Campestris) and Radish (Raphanus sativus). *Phyton (Austria)* 45: 229–235

Yue-ming B, Chun-yi W, Min W, Jian-ping G (2004) Influences of different ozone concentrations and fumigation days on Spinach growth and yield. *Sci Agric Sinica* 37: 1971–1975

Plant Biotechnology

High speed and high precision optical interferometric technique to investigate instantaneous growth related changes of plant leaves

Bodhipaksha Lalith Sanjaya Thilakarathne, Uma Maheswari Rajagopalan, Hirofumi Kadono, TetsushiYonekura

S1. Fundamental statistical properties of the speckle field and the effect of non-spatial uniformity of object

Speckles appear as a result of random interference of the scattered light by a rough surface object under the illumination of a coherent light such as a laser beam. The speckles were considered as a noise in the early advent of lasers. However, as theoretical interpretation of the laser speckle phenomenon developed, this phenomenon was widely recognized as an information source for the object under illumination. A large number of its applications were proposed and developed, e.g., surface roughness measurements, speckle velocimetry, stellar speckles, speckle interferometry, etc. The technique has also been applied for biological objects, e.g., blood flow measurements. These noninvasive measurement techniques using speckles have made them important making them no longer a random noise. Due to the randomness, it is important that a brief description on the statistical properties of the speckles (Dainty, 1984) becomes totally necessary for an interested reader to understand the basics of the technique used here in SIT (statistical interferometric technique).

In general, a speckle field is described as a complex optical field with an amplitude and a phase. In SIT, the statistical property of a fully developed Gaussian speckle field, i. e., a uniform probability density function of the speckle phase is utilized. Such a speckle field also shows related properties that the probability density function of the speckle intensity takes a negative exponential function resulting in the speckle contrast unity, C=1. In order to generate such a fully developed speckle field, only two conditions are needed to be satisfied. One is related to the optical roughness σ_o of the object and the other is related to the correlation length ξ of the surface height variations. The optical roughness σ_o, standard deviation of optical path variation due to surface height variation of the object, must be larger than the wavelength of the light used in the system. In our case, as a reflection setup was used, the surface roughness σ_h, standard deviation of the surface height variation of the object, must be larger than half of the wavelength of the

light used. Therefore in the optical setup shown in Figure S1, the main condition that needs to be fulfilled is that the roughness is,

$$\sigma_o >> \lambda \quad or \quad \sigma_h >> \lambda / 2 \tag{S1}$$

With respect to the correlation length that quantifies surface height variations, the number of scatterers N based on the discrete scatterer model is commonly introduced. N is the number of the scatterers contributing to the formation of the speckle field and is defined by

$$N = \frac{\text{area of illumination}}{\text{area of elementary scatterer}} = \frac{\pi w^2}{\pi \xi^2}, \tag{S2}$$

where w is the radius of the probing beam, and ξ is the correlation length of the surface height variations.

Our method is based on the statistics of Gaussian speckle field, the discussion has been restricted to Gaussian speckle field. In other words this means the complex speckle amplitude obeys Gaussian statistics according to the central limit theorem. In practice, this requirement is well satisfied with the condition,

$$N > 10. \tag{S3}$$

Here, let us define the j-th elementary wave from j-th scatterer contributing to the formation of the speckle field at a certain observation point P be a_j. The complex speckle amplitude A at the observation point P in a diffraction field (Figure S1) is given by,

$$A = A_r + iA_i = \sum_{j=1}^{N} a_j = \sum_{j=1}^{N} \left| a_j \right| \exp\left(i\phi_i \right). \tag{S4}$$

Here, suffixes r and i denote real and imaginary parts of the complex number, respectively. When both of the conditions given by Eqs.(S1) and (S3) are

satisfied, the statistics of the complex speckle amplitude becomes zero-mean circular Gaussian statistics. This means,

$$\begin{aligned} &< A >=< A_r > + i < A_i >= 0, \\ &\sigma_r = \sigma_i, \\ &\rho = < A_r A_i > \Big/ \sqrt{\sigma_r \sigma_i} = 0. \end{aligned} \tag{S5}$$

In Eq.(S5), <…> stands for ensemble average. σ_r and σ_i are the standard deviations of the real and imaginary parts of the complex speckle amplitude of A, respectively. ρ is the correlation coefficient of the real and imaginary parts of the complex speckle amplitude. In general, first order statistics of the Gaussian speckle field is described perfectly by means of the joint probability density function $p_{r,i}(A_r, A_i)$ of real and imaginary parts of the complex speckle amplitude, and takes two dimensional Gaussian distribution on the complex amplitude plane of A_r and A_i as shown in Figure S2. When the conditions of Eqs.(S1) and (S3) are satisfied, one can see that the contour line of a certain value of the probability density, i.e., equi-probability density ellipse, becomes circular.

When the optical roughness is smaller and does not satisfy the condition of Eq.(S1), so called partially developed speckle field is produced. Although the statistics of the complex speckle field sill obeys Gaussian statistics with the condition of Eq.(S3), the mean $<A>$ and the correlation ρ take certain values, and σ_r and σ_i are not equal in general. This implies that the equi-probability density ellipse deviates from the origin and becomes elliptic. The statistics of such a speckle field is called non-circular Gaussian statistics. The significant point of the partially developed speckle field is that its statistical properties are dependent on the surface roughness and the number of scatterers N. In other words, the speckle contrast and the probability density distribution of the speckle phase are dependent on those two parameters in very complex manner (Kadono and Asakura, 1985; Kadono, 1986).

However, the roughness becomes larger and satisfies the condition of Eq.(S1), the dependence of the speckle field on N becomes weaker and weaker.

Finally when the condition of the roughness given by Eq.(S1) is satisfied, the statistics of the speckle field does not depend on these parameters, σ_o and N. Therefore the fully developed speckle field is a very stable and a kind of saturated field.

In addition, the discussion above is the case that illumination and the observation directions are parallel and normal to the object surface where a specular reflection from the object is superposed onto the scattered component. As in the optical system used in our experiment, we observed the speckles in off axial diffraction field. In this case, as the observation direction deviates from the normal to the object surface, the speckle field quickly approaches to the fully developed speckle field even if the optical roughness of the object doesn't satisfy the condition of Eq.(S1). A detailed theoretical analysis of the statistical properties of the off axis diffraction speckle field is given in our previous study (Kadono, 1986). Although the wheat flour was not homogenized, due to the large optical roughness of the wheat layer together with the off-axis observation, the statistics of the field where SIT is based on was never affected by the spatial non-uniformity of the grain of wheat flour in practice. This was well coincide with the experience in our experiment.

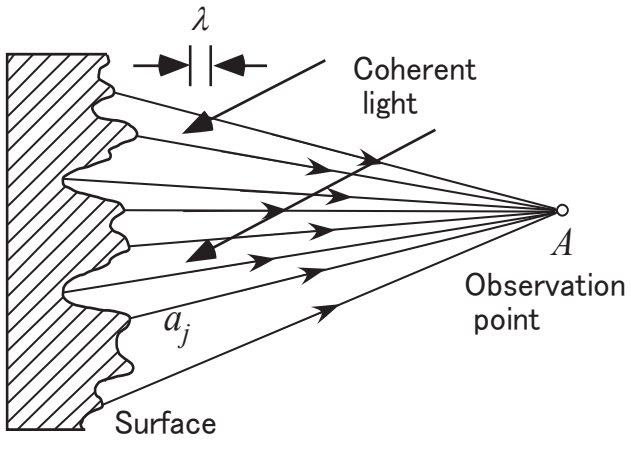

FigureS1 Complex speckle amplitude in diffraction field.

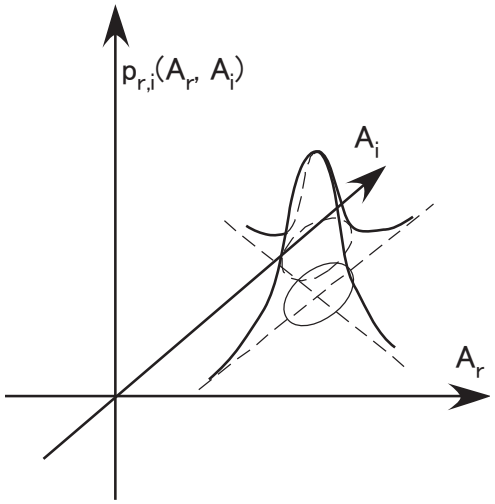

FigureS2 Joint probability density distribution of complex speckle amplitude

S2. Algorithm of Statistical Interferometry

In the optical system shown Figure 1A, the random speckle interference patterns corresponding to the elongation, Δx, of the object are stored in a frame memory through the CCD camera as $I(x,t_1), I(x,t_2), \cdots, I(x,t_n)$, at times $t = t_1, t_2 \cdots t_n$. Phasors corresponding to the phase change due to the elongation of the object are shown in Figure S3.

Next, we consider three images, $I_1(\mathbf{x})$, $I_2(\mathbf{x})$, $I_3(\mathbf{x})$, that are arbitrarily chosen from the frame memory, respectively, at times $t=h_1$, h_2, and h_3. The intensity distributions of those three random interference patterns are expressed by,

$$\begin{aligned} I_1(\mathbf{x}) &= I_0(\mathbf{x})\left[1+\gamma(\mathbf{x})\cos\left(\phi(\mathbf{x})+\psi_1\right)\right], \\ I_2(\mathbf{x}) &= I_0(\mathbf{x})\left[1+\gamma(\mathbf{x})\cos\left(\phi(\mathbf{x})\right)\right], \\ I_3(\mathbf{x}) &= I_0(\mathbf{x})\left[1+\gamma(\mathbf{x})\cos\left(\phi(\mathbf{x})+\psi_3\right)\right], \end{aligned} \tag{S6}$$

where $I_0(\mathbf{x})$ and $\gamma(\mathbf{x})$ are, respectively, the average intensity and the modulation factor at each point $\boldsymbol{x}$ on the observation plane. ψ_1 and ψ_3 are object phase difference between $t=h_1$ and h_2, and $t=h_2$ and h_3, respectively, and those values are to be derived.

Here, we briefly describe the way to derive the object phase (Kadono *et al.* 2001). Since three systems of equations, Eq. (S6), have five unknown variables, I_o, γ, ψ_1, ψ_3, and ϕ, we cannot calculate ψ_1 and ψ_3 directly. In the next step, we assume a certain value for the phases ψ_1 and ψ_3 as,

$$-\psi_1 = \psi_3 = \psi_v. \tag{S7}$$

The phase term ψ_v is referred to as a virtual phase whose value can be chosen arbitrarily. The phase of the speckle field is derived from Eq.(S6) with the assumption of Eq. (S7) as,

$$\phi'(\mathbf{x}) = \tan^{-1}\frac{I_1(\mathbf{x}) - I_3(\mathbf{x})}{I_1(\mathbf{x}) + I_3(\mathbf{x}) - 2I_2(\mathbf{x})}\cdot\frac{\cos\psi_v - 1}{\sin\psi_v}. \tag{S8}$$

$\phi'(x)$ is referred to as an evaluated phase of the speckle field. The assumption given by Eq.(S7) is not reasonable in general. As $\phi'(x)$ differs from the true phase $\phi(x)$of speckle field, the PDF of the evaluated phase $\phi'(x)$ of the speckle field doesn't take the uniform distribution of $1/2\pi$. This implies that, by making a proper correction for the assumption of Eq.(S7) based on the deviation of the PDF of the evaluated phase of speckle field from the uniform distribution, the actual object phase can be derived. The deviation from the uniform distribution becomes prominent even for a fairly small phase difference from the virtual phase value ψ_v for the object phase. To explain more precisely, two phase components, symmetrical $\Delta\psi_s$ and antisymmetrical phase deviations $\Delta\psi_a$, are introduced. Using these variables the object phase can be expressed by,

$$\begin{aligned} \psi_1 &= -\psi_v - \Delta\psi_s + \Delta\psi_a, \\ \psi_3 &= \psi_v + \Delta\psi_s + \Delta\psi_a. \end{aligned} \tag{S9}$$

According to the precise analysis, the symmetrical and the antisymmetrical deviations from the virtual phase cause nonuniform deviations expressed with $\cos 2\phi'$ and $\sin 2\phi'$ into the PDF of the evaluated phase of speckle field, respectively. These two types of deviation from the uniform PDF gives us a way to determine two phase components, $\Delta\psi_s$ and $\Delta\psi_a$,. Thus the object phases, ψ_1 and ψ_3, can be uniquely determined. Through changing the combination of three frames and repeating the same procedure, whole phase change of the object can be obtained.

The advantage of the method is that, because of the statistical basis of the method, improvement of the accuracy is inherently assured by taking more data samples into account, and the accuracy of $\lambda/1000$ can be easily achieved with approximately 40000 samples of data according to the computer simulation. However, the elongation of the object that can be determined has been limited to phase range less than 2π.

Dainty JC. 1984. *Laser Speckle and Related Phenomena (Topics in Applied Physics)*. Berlin: Springer-Verlag.

Kadono H, Asakura T. 1985. Statistical properties of the speckle phase in the optical imaging system. *Journal of Optical Society of America A* **2**, 1787-1792.

Kadono H, Takai, N.and Asakura, T. 1986. Statistical properties of the speckle phase in the diffraction region. *Journal of Optical Society of America A* **3**, 1080-1089.

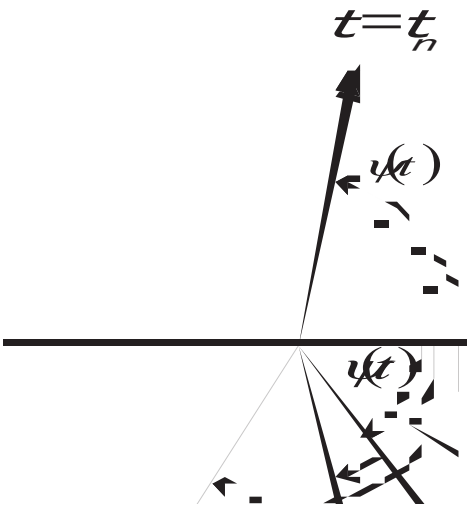

FigureS3 Phasors corresponding to the phase changes that are due to the elongation of the object

S3. Expansion of dynamic range in statistical interferometry

First we describe the practical procedure to acquire the interference patterns for obtaining the object phase as described in the previous section, and then the dynamic range of the measurement is expanded by improving the algorithm (Kobayashi and Kadono, 2010).

The reference interference patterns, I_1 and I_3, are acquired by introducing appropriate phase modulations $-\psi_r$ and $+\psi_r$ between the two illuminating beams through the use of a phase modulator (PZT). The phase modulation of $\pm\psi_r$ are introduced only at the beginning to assure the phase difference between three frames in combination because the combination of the very close phasors increase the error. Those phase modulations are shown in Figure S4A by using phasors.

The interference patterns due to the object elongation are recorded continuously in a frame memory. The phase due to the object change at time t_i of i-th frame is indicated by $\angle\mathrm{Phasor}_{2,\mathrm{i}}$, and the interference speckle pattern at time t_i is denoted by $I_{2,i}$. Therefore, the phase difference between the reference patterns and the initial object phase are given by,

$$\begin{aligned}\angle\mathrm{Phasor}_1 &= \angle\mathrm{Phasor}_{2,1} - \psi_r,\\ \angle\mathrm{Phasor}_3 &= \angle\mathrm{Phasor}_{2,1} + \psi_r.\end{aligned} \tag{S10}$$

$\angle\cdots$ shows the angle of the phasor. The object phase is calculated from the combination of three frames of $I_{2,i}$ with I_1 and I_3 fixed. The object phase change $\Delta\psi(t_i)$ at t_i is given with the explicit indication of the combination of three interference patterns as;

$$\Delta\psi(t_i) = \psi(t_i)\big|_{I_1, I_{2,i}, I_3} - \psi(t_1)\big|_{I_1, I_{2,1}, I_3},\ (i = 1, 2, 3\cdots n). \tag{S11}$$

Here, n is the number of the interference patterns acquired for the object. The object elongation is given by, $\Delta x(t_i) = \Delta\psi(t_i)\lambda / 2\pi \sin\theta$.

If the $\text{Phasor}_{2,i}$ is not close to the reference Phasor_1 or Phasor_3, the object phase can be obtained with a fairly small error. As the $\text{Phasor}_{2,i}$ approaches very close to the reference Phasor_1 or Phasor_3, the error in the calculated object phase would become larger because the difference in the interference pattern becomes smaller. In addition, the object phase error also increases when the decorrelation between $I_{2,i}$, I_1 ,and I_3 occurs due to either translation of object or change of surface structure.

Therefore, when the object phase $\Delta\psi(t_k)$ exceeds a certain threshold ψ_{th} , i.e. $\Delta\psi(t_k) \geq \psi_{th}$, the reference patterns of Phasor_1 or Phasor_3 have to be renewed as I_1' and I_3' using the phase modulator with the modulation $\pm\psi_r$ for $\text{Phasor}_{2,k}$ (Figure S4B). The renewed phasors satisfy the following relations:

$$\begin{aligned} \angle\text{Phasor}_1' &= \angle\text{Phasor}_{2,k} - \psi_r, \\ \angle\text{Phasor}_3' &= \angle\text{Phasor}_{2,k} + \psi_r. \end{aligned} \tag{S12}$$

Therefore, the object phase at t_j, after the renewal of the reference pattern is given by,

$$\Delta\psi'(t_j) = \psi(t_{k+j})\big|_{I'_1, I_{2,(k+j)}, I'_3} - \psi(t_k)\big|_{I'_1, I_{2,k}, I'_3}, \ (j = 1, 2, 3 \cdots n-k). \tag{S13}$$

Then, corresponding elongation after the renewal is given by,

$$\Delta x'(t_j) = \Delta\psi'(t_j)\lambda / 2\pi \sin\theta. \tag{S14}$$

The total object elongation at time t_i, (i=k+j), is expressed by,

$$\Delta x(t_i) = \Delta x(t_k) + \Delta x'(t_j) \ . \tag{S15}$$

The renewal of the reference patterns are also carried out when the number of invalid phase data exceeds a certain threshold, and the modulation factor $\gamma(\mathbf{x})$ does not satisfy a given threshold. One of the reason for the invalid phase data is the decorrelation of the speckle patterns.

When the condition $\left|\Delta\psi'(t_j)\right| < \psi_{th}$ does not hold again, the reference patterns are renewed. In practice, the threshold ψ_{th} was set to be fairly smaller value of $2\pi/10$ that corresponds to the elongation of the object 0.17μm with the observation angle θ=22 degree. This resulted in the frequent renewal of the reference speckle patterns. By repeating the renewal of the reference patterns, the algorithm made it possible to measure the phase changes of the object that were much larger than 2π with robustness to speckle decorrelation and unexpected external turbulence. In addition, the data processing unit of the measurement software was designed so as to continuously monitor the invalid data points in the acquired images and report the number of invalid data points which were mainly due to the decorrelation of speckle patterns and electrical noise. In this way, we could monitor and assure the quality of measurements and data acquisition.

Kobayashi K, Kadono H. 2010. Expansion of the dynamic range of statistical interferometry and its application to extremely short- to long-term plant growth monitoring. *Appl. Opt.* **49**, 6333-6339.

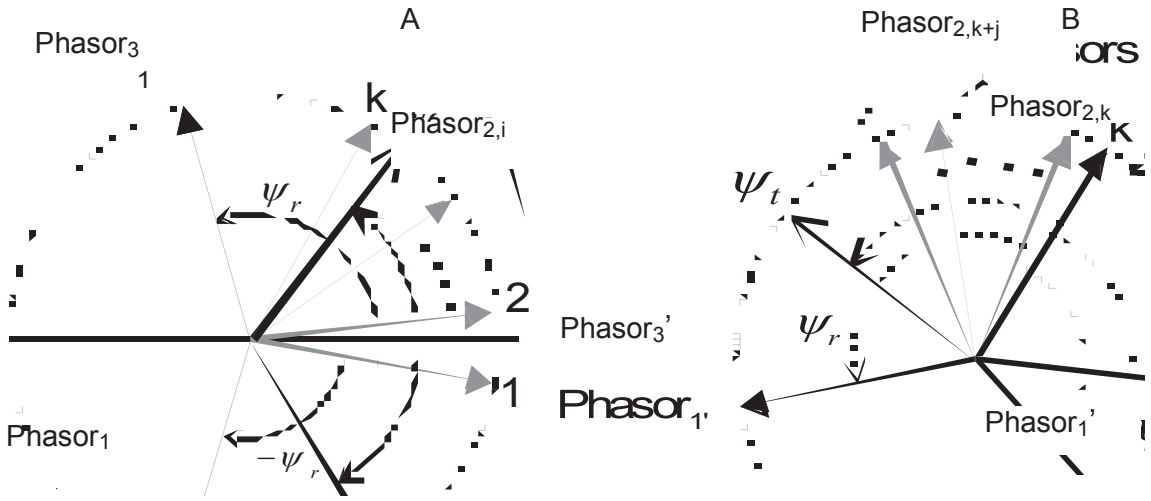

FigureS4 Expansion of the dynamic range,(a) before, and (b) after renewal of reference patterns, $Phasor_1$ and $Phasor_3$.

S4. Effect of translation and change of surface profile of the object on the speckle pattern

Here, the decorrelation of individual speckle pattern as the plant grows is considered. There are two cases that can cause decorrelation between the speckle patterns as illustrated in Figure S5. One is due to the translation of the object with keeping the surface height profile (Figure S5A). The other one is due to the change of the surface profile itself (Figure S5B). In former case, when the distance of the lateral translation Δx exceeds $2w$, that is the probing beam diameter, the correlation between the speckle patterns before and after the translation is completely lost. Therefore, the important parameter to preserve the correlation of the speckle patterns is the ratio of the lateral translation and the diameter of the probing beam. It should be noted that we are concerned with the very short-term growth dynamics of the plant, and the elongation rate is determined from the observation over 5.5 sec. The translation over this period is a few hundreds nm at most and is negligibly smaller than the probing beam diameter of 770μm. As for the latter case, the effect is also negligibly small due to the relatively short observation period to measure elongation rate over 5.5 sec.

As for the observation for relatively longer period, the frequent renewal of the reference speckle patterns could solve the problem of the decorrelation of the speckle patterns.

The surface of the leaf was covered with the wheat flour layer to suppress the generation of the biospeckles. A slight displacement of the wheat grain might introduce the decorrelation of the speckle patterns in practice. The grain size of the wheat flour is ranging from a few μ□ to tens of μm. The speckle patterns are formed as a result of an interference of overall contributions of elementary waves from the scattering points under illumination. Therefore, within the illuminated area, any macroscopic irregular movements of a few grains among enormous number of wheat flour grains need not necessarily cause a significant decorrelation of the speckle pattern.

To examine the actual decorrelation of the speckle patterns, we acquired individual speckle patterns at a sampling rate of 1 sec, and calculated the cross-correlation coefficient of the speckle patterns with the initially obtained one for mature and young rice plants. Figure S6 shows the result over 4 min. A slight decorrelation can be observed as a function of time. However, the correlation coefficient is well maintained within 1 to 0.9 over 4 min. and 1 to 0.99 over 10 sec., which is small enough since the growth rate is determined from the measurements over 5.5 sec.

As for the minute change of surface structure that may occur for the longterm measurements and may result in the decorrelation of the speckle pattern, this problem is solved due to the frequent renewal the of the reference speckle patterns as already described in the Supplementary Material S3.

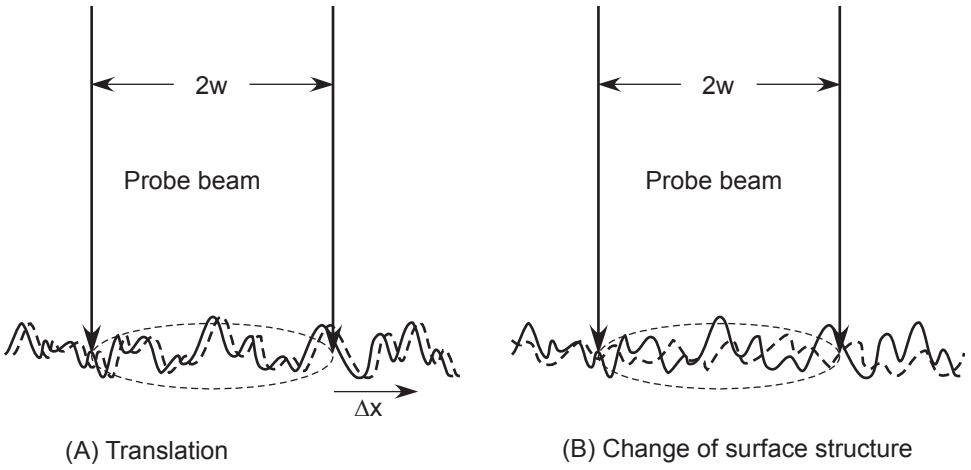

FigureS5 Decorrelation of speckle patterns

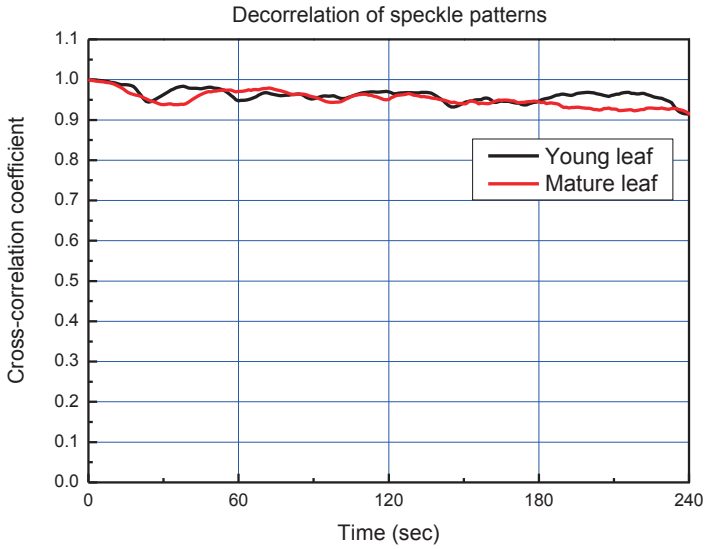

FigureS6 Decorrelation of speckle patterns for mature and young leaf

S5 Effect of wavelength of probing beam leakage

Even though the leaked power of the probing beam was fairly small, i.e., 2% of the incident beam or 9 μw, the wavelength 633 nm of He-Ne laser is very close to the absorption band of chlorophyll b. In order to confirm the effect of the leakage of the probing beam, additional experiments were performed.

First,we conducted ozone exposure experiment with YAG-SHG (CL532-100-S, CrystaLaser, USA) laser of wavelength 532 nm. The experimental results showed the same tendency with those obtained using the probing beam of wavelength 633nm. Figure S7 shows one of the experimental results for Fusaotome rice plant under 240 ppb ozone exposure, and it showed around 20% reduction.

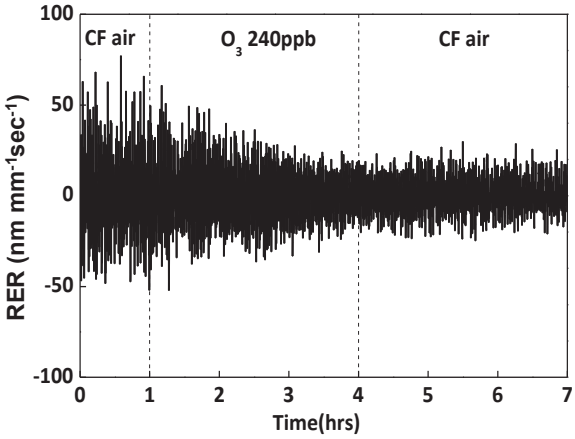

Fig. S7 NIF of Fusaotome under 240ppb ozone exposure with probing beam of 532nm.

S6 Effect of leakage of probing beam

To examine the effect of leakage of the probing beam (633 nm) on elongation rate measurements, another laser light (a laser diode of wavelength 635 nm) to provide additional illumination from the back side of the leaf were prepared. The power of the additional beam was adjusted to be double of the leaked power *Pt* of the probing beam of 633 nm. Then the additional beam was turned on and off at an interval of two hours. One of the experimental results is shown in Figure S8. As a result, we could not see any significant effect of the additional illumination on the dynamic growth behavior of the plant at the wavelength 635 nm.

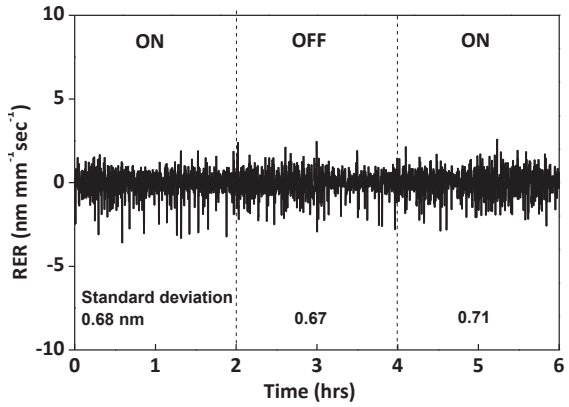

Figure S8 Change of NIF under additional light illumination